Ultrafast laser and swift heavy ion irradiation: Response of Gd_2O_3 and ZrO_2 to intense electronic excitation

Dylan R. Rittman,[1,2] Cameron L. Tracy,[3] Alex B. Cusick,[3] Michael J. Abere,[3] Ben Torralva,[4] Rodney C. Ewing,[2] and Steven M. Yalisove[3]
[1]*Department of Nuclear Engineering and Radiological Sciences, University of Michigan, Ann Arbor, Michigan 48109, USA*
[2]*Department of Geological Sciences, Stanford University, Stanford, California 94305, USA*
[3]*Department of Materials Science and Engineering, University of Michigan, Ann Arbor, Michigan 48109, USA*
[4]*Department of Atmospheric, Oceanic and Space Sciences, University of Michigan, Ann Arbor, Michigan 48109, USA*

(Received 21 February 2015; accepted 23 April 2015; published online 30 April 2015)

In order to investigate the response of materials to extreme conditions, there are several approaches to depositing extremely high concentrations of energy into very small volumes of material, including ultrafast laser and swift heavy ion (SHI) irradiation. In this study, crystalline-to-crystalline phase transformations in cubic Gd_2O_3 and monoclinic ZrO_2 have been investigated using ultrafast laser irradiation. The phases produced by the extreme conditions of irradiation were characterized by grazing incidence x-ray diffraction (GIXRD) and Raman spectroscopy. Gd_2O_3 exhibited a cubic-to-monoclinic phase transformation, as evidenced by the appearance of the monoclinic $(40\bar{2})$, (003), (310), and $(11\bar{2})$ peaks in the GIXRD pattern and of four A_g and three B_g Raman modes. ZrO_2 underwent a monoclinic-to-tetragonal phase transformation, as evidenced by the emergence of the tetragonal (101) peak in the GIXRD pattern and of E_g and A_{1g} Raman modes. The new phases formed by ultrafast laser irradiation are high temperature polymorphs of the two materials. No evidence of amorphization was seen in the GIXRD data, though Raman spectroscopy indicated point defect accumulation. These results are identical to those produced by irradiation with SHIs, which also deposit energy in materials primarily through electronic excitation. The similarity in damage process and material response between ultrafast laser and SHI irradiation suggests a fundamental relationship between these two techniques. © *2015 AIP Publishing LLC*.
[http://dx.doi.org/10.1063/1.4919720]

The response of materials to swift heavy ion (SHI) irradiation is critical to understanding the behavior of materials in a range of extreme environments. However, SHI irradiations are both costly and time consuming due to limitations on available beam time at SHI beam facilities. We have investigated the use of ultrafast laser irradiation as an efficient, low cost surrogate for SHI irradiation. The similar mechanisms and timescales of damage[1–4] provide a strong basis for comparison of the two irradiation techniques.[3,4]

The nature of energy deposition is similar as ultrafast lasers and SHIs both excite electrons through their electric fields[5,6]—the difference being that the laser produces an oscillating field while the SHI is a moving point charge. While SHIs excite electrons of an insulator through a relatively simple process of inelastic collisions caused by its electric field, the process of excitation in an insulator due to ultrafast laser irradiation is more complex. Initial excitation is caused by a combination of tunneling and multiphoton ionization that compete against one another with multiphoton ionization dominating at low fluences and tunneling ionization dominating at high fluences.[7] Once a sufficient electron population exists in the conduction band, the insulating materials begins to absorb like a metal, where inverse Bremsstrahlung leads to free electrons with even higher energies.[8] At this point, an avalanche occurs through impact ionization, further populating the conduction band.[7]

Ultrafast lasers modify materials in the near surface with spots tens of microns wide and depths only tens to hundreds of nm deep.[9] This contrasts with SHIs, which produce tracks microns long but only 3–10 nm wide.[2] However, both techniques have been shown to produce energy density dependent damage morphologies.[2,10]

The energy densities resulting from these processes are comparable, though there is a stark difference in energy gradient due to the orders of magnitude different diameters of the damage spots. Simulations of SiO_2 irradiation with 11.4 MeV/nucleon Ca ions have shown that 100 fs after SHI interaction, electron energy density is over 1000 eV/nm^3 in the track's center. It then drops off rapidly to 1 eV/nm^3 at a radius of 1 nm, at which point it deceases much more gradually to 0.1 eV/nm^3 at a radius of 10 nm. Irradiation of SiO_2 with an ultrafast laser at fluences of 40 J/cm^2 leads to electron energy densities on the order of 100s of eV/nm^3 in the spot's center after similar time delays.[4]

Although there are differences in energy deposition, damage geometry, and energy density, the response of materials to ionizing radiation will be the same as long as the timescales of energy deposition are similar. Critically, like SHIs, the duration of energy deposition by ultrafast lasers is shorter than the recombination time of electrons. This is different from nanosecond lasers that repeatedly cycle electrons from the valance band to the conduction band throughout the pulse duration.[11]

Promotion of electrons from the valance band (bonding state) to the conduction band (anti-bonding state) leads to the weakening of bonds in ionic-covalent materials since bonding in these materials depends on valance electrons. Thus, bond-weakening leads to a change in the interatomic potentials on sub-picosecond timescales,[12–19] which can lead to the production of point defects in the form of interstitials and vacanciees.[15] Electron-hole pair recombination leads to electron-phonon coupling from 1 to 10 ps.[1,17–20] If this phonon generation heats the material to a sufficiently high temperature, then a shock wave will propagate through the material from 20 to 100 ps.[1,2,17] The role of these three mechanisms—bond-weakening, electron-phonon coupling, and shock wave propagation–in the overall damage process is still much debated.[17,18]

Gd_2O_3 and ZrO_2 are two materials of interest when studying SHI-material interactions. Gd_2O_3, used as a burnable poison in nuclear fuel, is continuously exposed to energetic fission fragments. Because of this, it is important to understand its behavior under SHI irradiation. ZrO_2 is only used in nuclear applications when it is stabilized in its cubic polymorph by yttrium oxide. However, extensive analyses have been performed on the response of pure monoclinic ZrO_2 to SHI irradiation,[21–23] which makes it an excellent candidate for the analysis and comparisons in this study.

The goal of this letter is to investigate the response of Gd_2O_3 and ZrO_2 when subjected to intense electronic excitation from ultrafast laser irradiation. The significant finding is that the material response to ultrafast laser irradiation—cubic-to-monoclinic and monoclinic-to-tetragonal phase transformations in Gd_2O_3 and ZrO_2, respectively, along with evidence of point defect accumulation and no evidence of amorphization—is consistent with the response of these materials to SHI irradiation.[21–28] Furthermore, we show that ultrafast lasers may be a useful alternative to SHI irradiation from both a practical and theoretical standpoint: practical in the sense that irradiation by ultrafast lasers may provide for relatively rapid screening of novel materials before more difficult SHI irradiations are completed; and theoretical in the sense that ultrafast laser irradiations can provide insights into the physical mechanisms underlying the radiation response of materials to SHI irradiation.

Polycrystalline samples of cubic Gd_2O_3 and monoclinic ZrO_2 were sintered in stagnant air at ambient pressure. Gd_2O_3 was heated at a rate of 60 K/h to 1333 K, held for 50 h, and cooled to room temperature at a rate of 60 K/h. ZrO_2 was heated at a rate of 60 K/h to 1313 K, held for 50 h, and cooled to room temperature at a rate of 60 K/h. Sintering produced pellets of 85% theoretical density with grain size of approximately 10 μm, which were sufficiently durable for handling throughout experiments. The samples were then irradiated in air at room temperature by a Clark MXR Ti:Sapphire 780 nm laser with a pulse duration of 150 fs, maximum pulse energy of 800 μJ, and maximum repetition rate of 1 kHz. The $1/e^2$ diameter of the focused spot was measured by a DataRay WinCamD beam profiler and was found to follow a Gaussian profile. The laser was focused onto the surface of the sample at normal incidence during irradiation. We report the peak fluence, which occurs at the spot's center. For context on the fluences used in the irradiations, the ablation threshold of ZrO_2 is 2.8 J/cm^2.[29] The threshold for Gd_2O_3 has not been determined, though it is likely comparable to that of ZrO_2 since the materials have similar band gaps.[30,31] Phase transformations were characterized by both grazing incidence x-ray diffraction (GIXRD) and Raman spectroscopy.

Samples analyzed by GIXRD were irradiated at 40 J/cm^2 with a single pass in a raster pattern and 50% overlap of adjacent damage spots. Irradiation of a large surface area was necessary as GIXRD intrinsically uses a large spot size. GIXRD was performed using a Rigaku Ultima IV X-Ray Diffractometer, using Cu K_α x-rays and an incident angle of 0.8° for ZrO_2 and 2° for Gd_2O_3. The increased x-ray absorbance of Gd, as compared with Zr, allowed for the use of a higher incident angle while maintaining similar penetration depth normal to the irradiated surface. It is calculated that approximately 95% of the incident x-rays were scattered in the first 400 nm of material.[32] The detector was set to scan in steps of 0.03° at a rate of 0.025° per minute.

Samples analyzed by Raman spectroscopy were irradiated at fluences between 5 and 60 J/cm^2 (per shot) and 10 (fully overlapping) shots for Gd_2O_3 and at 0.50 J/cm^2 and between 10 and 10^5 shots for ZrO_2. For spots irradiated with 10 shots, a repetition rate of 1 Hz was used. For spots irradiated with 10^2–10^3 shots, a repetition rate of 100 Hz was used. For spots irradiated with 10^4 shots or more, a repetition rate of 1 kHz was used. Varying the repetition rate was done in order to reduce the error in shot number. A Renishaw Raman spectrometer operating at 633 nm was used for analysis of Gd_2O_3 irradiations. Results from ZrO_2 irradiations were analyzed by a Spex Raman spectrometer operating at 532 nm. The 532 nm spectrometer was used in order to collect data on ZrO_2's E_g Raman mode, which was not accessible using the 633 nm spectrometer. Using the extinction coefficient to calculate absorption depth, it is found that approximately 90% of incident Raman laser light is absorbed in the first 35 μm of material.[33] Due to the large depth that the Raman probe interrogates, it was necessary to irradiate the samples with multiple pulses in the same region so a sufficiently large volume of transformed material could be created.

Figure 1 shows GIXRD results for Gd_2O_3 and ZrO_2 both before and after exposure to the laser. Both patterns show that, within the volume probed by the x-rays, both low and high temperature polymorphs coexist. This suggests that either an incomplete transformation within the region modified by the laser or an x-ray penetration depth greater than that of the laser such that signal is obtained from both the irradiated volume and the unirradiated bulk below.

The formation of the monoclinic phase in Gd_2O_3 is evidenced by the appearance of $(40\bar{2})$, (003), (310), and $(11\bar{2})$ peaks in Fig. 1(a). There is some evidence of the (111) and (401) monoclinic peaks as well, evident as shoulders on the cubic (222) peak, though they are obscured by its high intensity. Similarly, the formation of the tetragonal phase in ZrO_2 is supported by the appearance of the (101) peak in Fig. 1(b). The (002) and (200) tetragonal peaks are both low intensity and closely overlap with the (002) and (200) monoclinic peaks, respectively, and are therefore not clearly distinct in these diffraction patterns. However, the shift in peak position

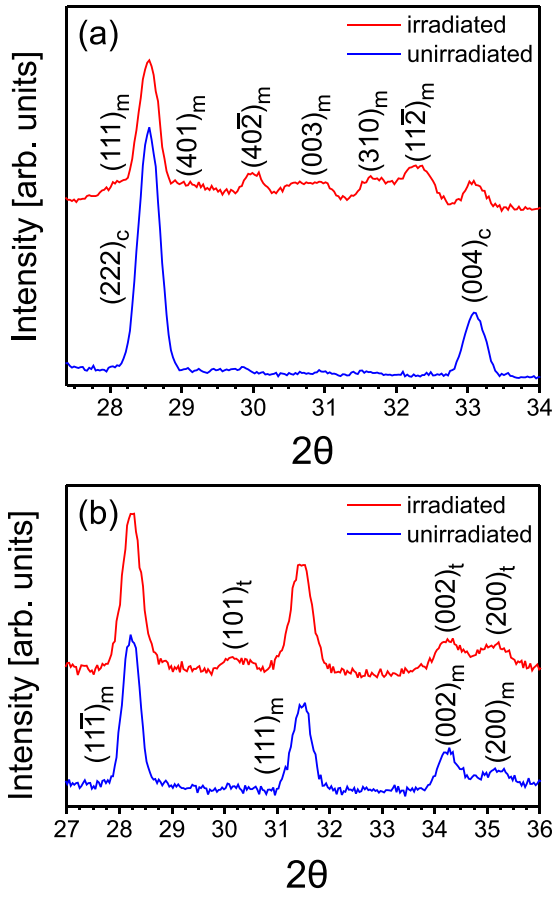

FIG. 1. GIXRD results showing (a) the cubic-to-monoclinic transformation in Gd_2O_3 and (b) the monoclinic-to-tetragonal transformation in ZrO_2. Subscripts of indices indicate the phase (c = cubic, m = monoclinic, and t = tetragonal). Irradiations were performed at 40 J/cm^2 with a single pass in a raster pattern and 50% overlap of adjacent damage spots.

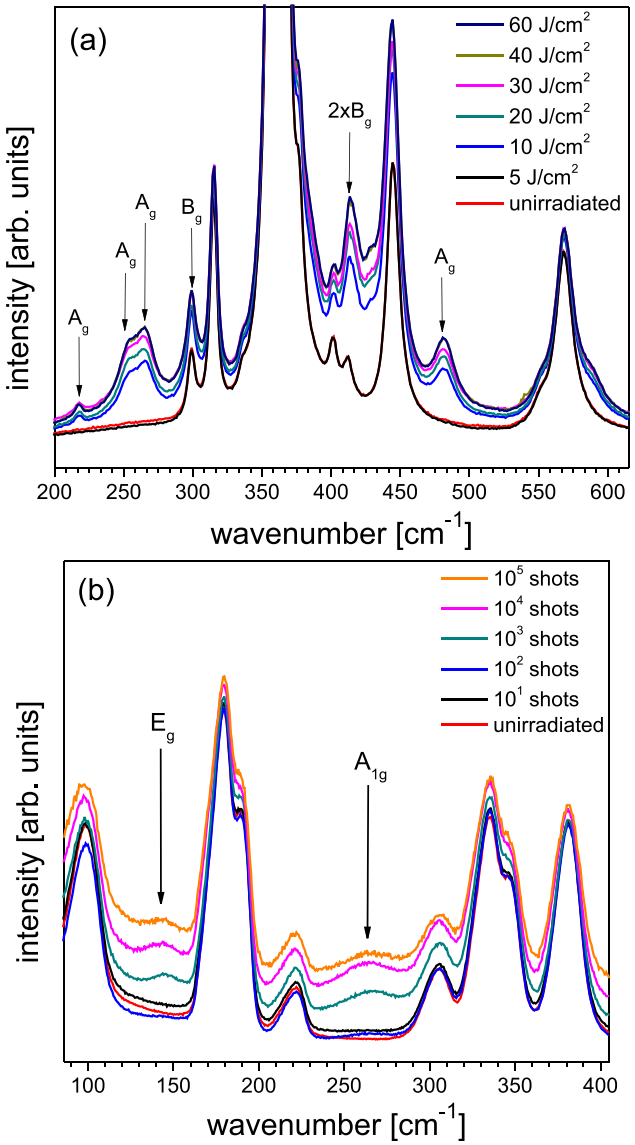

FIG. 2. Raman spectroscopy results showing (a) the cubic-to-monoclinic transformation in Gd_2O_3 and (b) the monoclinic-to-tetragonal transformation in ZrO_2. Irradiation of Gd_2O_3 was performed between 5 and 40 J/cm^2 for 10 shots. Irradiation of ZrO_2 was performed at 0.50 J/cm^2 for between 10 and 10^5 shots.

and change in relative intensities of the two features, which are likely combinations of the initial and new phase peaks, provides further confirmation that the phase transformation occurred. For both materials, there is no evidence of amorphization in the form of low intensity x-ray scattering over a broad low 2θ range. This is consistent with results from SHI irradiation studies.[21,24,26,28]

For ZrO_2, the (101) tetragonal peak closely overlaps with the (111) peak of the fluorite structure, another high temperature polymorph. For Gd_2O_3, multiple peaks in the spectrum overlap with either the high pressure or high temperature hexagonal polymorph. Raman spectroscopy was used to further differentiate between the different polymorphs in both materials, confirm the observations from the GIXRD data, and provide information on the effect of ultrafast laser irradiation on short-range order.

Raman spectroscopy confirmed the cubic-to-monoclinic phase change in Gd_2O_3 and the monoclinic-to-tetragonal phase change in ZrO_2 (Fig. 2). The emerging four A_g and three B_g modes in Fig. 2(a) illustrate the cubic-to-monoclinic phase change in Gd_2O_3.[34] Likewise, the emerging E_g and A_{1g} modes in Fig. 2(b) illustrate the monoclinic-to-tetragonal phase change in ZrO_2.[35] These data remove any ambiguity associated with the phase identification from the GIXRD results. The two order of magnitude with larger penetration depth in Raman spectroscopy as compared with GIXRD explains the lack of initial phase peak intensity reduction in the post-irradiation Raman spectra.

High temperature polymorph Raman signals were only found for Gd_2O_3 at high fluences (>5 J/cm^2). The monoclinic Raman modes do not appear at 5 J/cm^2, but then appear and increase in intensity at fluences from 10 to 40 J/cm^2. Finally, the intensity of the monoclinic Raman modes saturates from 40 to 60 J/cm^2, as indicated by the overlapping data. The absence of a tetragonal ZrO_2 Raman signal at high fluence is probably not associated with a low volume of transformed material as compared with the penetration depth of the Raman laser since a wide variety of fluence and shot number combinations were attempted in the high fluence regime without detecting the Raman signal. Furthermore, the Raman signal in irradiated monoclinic Gd_2O_3 was detected over a range of high fluence irradiation conditions, suggesting that the volume of tetragonal ZrO_2 should be sufficiently large to

produce a Raman signal even when compared with the large penetration depth of the Raman laser.

The absence of a tetragonal ZrO_2 Raman signal following high fluence irradiation would seemingly conflict with the GIXRD data, but XRD is sensitive primarily to long-range order while Raman spectroscopy reveals local structural features. Thus, this discrepancy might indicate the presence of significant strain or defect concentration in this phase at higher fluences that distorts the local structure. This interpretation is further supported by the increased background in the irradiated Raman data, which is indicative of defect accumulation. The loss of Raman signal corresponding to a given phase without accompanying loss of long-range structure, as evidenced by GIXRD results, is a common result in SHI irradiations of radiation-tolerant materials as irradiation-induced point defects tend to produce significant microstrain, distorting the local coordination of atoms.[36]

The Raman signal for tetragonal ZrO_2 appears in the lower fluence regime. The first evidence of tetragonal ZrO_2 is detected at 10^2 shots. As shots are increased to 10^3 and 10^4, signal intensity and background increase simultaneously. At 10^5 shots, background continues to increase, while the signal for tetragonal ZrO_2 decreases.

There is considerable debate about which damage mechanism drives phase transformations induced by SHI irradiation.[17,18,21–23] Models of phase transformations include the thermal spike,[21,22] where the SHI melts the local material and allows for a structural rearrangement into a new phase, and a strain-induced model, where the SHI creates dislocations in the material and the strain field drives the transformation.[23] Bond-weakening, which alters interatomic potentials, has also been proposed.[17,18] By "tuning" the fluence of the ultrafast laser one can change the dominant damage mechanism; thus, gaining insight into the physics underlying the transformation. This is not possible with SHI irradiation.

Distinct fluence regimes exist, in which either bond-weakening, melting due to electron-phonon coupling, or shock wave propagation is the dominant damage mechanism. The two thresholds that define these regimes are (1) the thermal melting threshold that defines the fluence necessary to thermally melt the material and (2) the shock melting threshold that defines the fluence necessary for the shock wave to generate dislocations.[37–39] For reference, the ablation threshold is in between the thermal and shock melt thresholds.

Bond-weakening dominates below the thermal melting threshold of the material since no dislocations are generated and the material's structure cannot rearrange due to melting. Thermal effects dominate in between the thermal and shock melting thresholds since the shock wave cannot produce dislocations, and any point defects generated by bond-weakening will be eliminated due melting. Dislocations produced by the shock wave become relevant above the shock melting threshold. Although thermal effects will still affect the near surface, the depth of this dislocation damage is deeper than damage generated by thermal effects.[39]

Phase transformations due to high fluence irradiation (Figs. 1 and 2(a)) are due to either thermal effects or shock wave propagation. The increasing intensity of the monoclinic Gd_2O_3 Raman signal with increasing fluence would be expected if melting or shock wave propagation was critical to the phase transformation; a higher fluence will melt a greater volume of material, and the material would be heated to a high temperature and thus generate a stronger shock wave. Both of these processes would cause a greater volume of material to transform.

The phase transformation induced by low fluence irradiation of ZrO_2 (Fig. 2(b)) was caused by irradiation below the melting threshold. Based on the electrical permittivity[40] and magnetic permeability[41] of ZrO_2, the electric field produced by irradiation at 0.5 J/cm^2 is calculated to be 6.0 MV/cm.[41] An electric field of over 15 MV/cm is needed to melt Si,[42,43] and greater electric fields are needed to cause damage in dielectrics than in Si.[42,44] Due to the sub-thermal melting threshold fluence, bond-weakening can be used to explain results seen in this scenario. Since bonds are weakened when incident radiation promotes electrons from the valance band to the conduction band, atoms are able to move about the lattice according to their room temperature thermal velocity,[16] and it has been suggested that this atomic motion can create point defects.[15] This point defect model can be extended to describe crystalline-to-crystalline phase transformations as well: accumulated strain from defects could drive the transformation or a more gradual process could occur where the atoms form a new crystalline structure instead of occupying interstitial sites.

The behavior of the tetragonal ZrO_2 Raman signal intensity as a function of shot number (Fig. 2(b)) is consistent with the bond-weakening model. Initially, a simultaneous increase in both Raman signal of tetragonal ZrO_2 and background would be expected as both point defects and tetragonal ZrO_2 are formed. Further increases in shot number, past the point where the ZrO_2 in the laser-matter interaction region is fully transformed, will increase background without a corresponding increase in the Raman signal of tetragonal ZrO_2.

Beyond the applications in this letter, the use of ultrafast lasers in SHI studies could be extended to ultrafast time-resolved x-ray diffraction experiments due to the large spot size and time resolution of the laser. Probing of materials at the atomic scale with ~50 fs resolution can shed light on the non-equilibrium phase transformation pathway in ways not possible with SHIs alone.

In summary, we have investigated the cubic-to-monoclinic and monoclinic-to-tetragonal phase transformations in Gd_2O_3 and ZrO_2, respectively, induced by ultrafast laser irradiation. These results were characterized by both Raman spectroscopy and GIXRD. Raman spectroscopy provided evidence of point defect accumulation. GIXRD revealed that the transformation could be induced without amorphizing a detectable amount of the material. The results determined for ultrafast laser irradiation are entirely consistent with the results from SHI irradiations. Furthermore, the underlying transformation mechanisms of ultrafast laser and SHI irradiation were shown to be the same. Overall, the ability of both ultrafast lasers and SHIs to rearrange and disorder structures through identical damage processes indicates a promising link between the two processes of depositing large amounts of ionizing energy into a material; thus, ultrafast laser irradiations can be used to complement SHI irradiations.

This work was supported by the Materials Science of Actinides Center, an Energy Frontier Research Center funded by the U.S. Department of Energy (DOE), Office of Science, Basic Energy Sciences (BES), under Award No. DE SC0001089 (GIXRD, Raman spectroscopy, and sample preparation), and by the Air Force Office of Scientific Research Contract No. FA9550-12-1-0465 (ultrafast laser irradiations at the University of Michigan).

[1]B. Rethfeld, K. Sokolowski-Tinten, D. Von der Linde, and S. I. Anisimov, Appl. Phys. A **79**, 767 (2004).
[2]J. Zhang, M. Lang, R. C. Ewing, R. Devanathan, W. J. Weber, and M. Toulemonde, J. Mater. Res. **25**, 1344 (2010).
[3]H. Y. Xiao, W. J. Weber, Y. Zhang, X. T. Zu, and S. Li, Sci. Rep. **5**, 8265 (2015).
[4]B. Rethfeld, A. Rämer, N. Brouwer, N. Medvedev, and O. Osmani, Nucl. Instrum. Methods Phys. Res., Sect. B **327**, 78 (2014).
[5]A. Kaiser, B. Rethfeld, M. Vicanek, and G. Simon, Phys. Rev. B **61**, 11437 (2000).
[6]M. A. Nastasi, J. W. Mayer, and J. K. Hirvonen, *Ion-Solid Interactions: Fundamentals and Applications* (Cambridge University Press, 1996).
[7]A. C. Tien, S. Backus, H. Kapteyn, M. Murnane, and G. Mourou, Phys. Rev. Lett. **82**, 3883 (1999).
[8]B. Rethfeld, A. Kaiser, M. Vicanek, and G. Simon, Phys. Rev. B **65**, 214303 (2002).
[9]D. Von der Linde and K. Sokolowski-Tinten, Appl. Surf. Sci. **154**, 1 (2000).
[10]T. H. R. Crawford, J. Yamanaka, G. A. Botton, and H. K. Haugen, J. Appl. Phys. **103**, 053104 (2008).
[11]V. I. Emel'Yanov and P. K. Kashkarov, Appl. Phys. A **55**, 161 (1992).
[12]C. V. Shank, R. Yen, and C. Hirlimann, Phys. Rev. Lett. **51**, 900 (1983).
[13]E. N. Glezer, Y. Siegal, L. Huang, and E. Mazur, Phys. Rev. B **51**, 6959 (1995).
[14]E. N. Glezer, Y. Siegal, L. Huang, and E. Mazur, Phys. Rev. B **51**, 9589 (1995).
[15]M. J. Abere, C. Chen, D. R. Rittman, M. Kang, R. S. Goldman, J. D. Phillips, B. Torralva, and S. M. Yalisove, Appl. Phys. Lett. **105**, 163103 (2014).
[16]A. M. Lindenberg, J. Larsson, K. Sokolowski-Tinten, K. J. Gaffney, C. Blome, O. Synnergren, J. Sheppard, C. Caleman, A. G. MacPhee, D. Weinstein *et al.*, Science **308**, 392 (2005).
[17]D. M. Duffy, S. L. Daraszewicz, and J. Mulroue, Nucl. Instrum. Methods Phys. Res., Sect. B **277**, 21 (2012).
[18]N. Itoh, D. M. Duffy, S. Khakshouri, and A. M. Stoneham, J. Phys.: Condens. Matter **21**, 474205 (2009).
[19]D. Von der Linde, K. Sokolowski-Tinten, and J. Bialkowski, Appl. Surf. Sci. **109**, 1 (1997).
[20]M. Toulemonde, Ch. Dufour, A. Meftah, and E. Paumier, Nucl. Instrum. Methods Phys. Res., Sect. B **166**, 903 (2000).
[21]A. Benyagoub, Phys. Rev. B **72**, 094114 (2005).
[22]A. Benyagoub, Nucl. Instrum. Methods Phys. Res., Sect. B **245**, 225 (2006).
[23]G. Baldinozzi, D. Simeone, D. Gosset, I. Monnet, S. Le Caër, and L. Mazerolles, Phys. Rev. B **74**, 132107 (2006).
[24]A. Benyagoub, F. Levesque, F. Couvreur, C. Gibert-Mougel, Ch. Dufour, and E. Paumier, Appl. Phys. Lett. **77**, 3197 (2000).
[25]A. Benyagoub, F. Couvreur, S. Bouffard, F. Levesque, C. Dufour, and E. Paumier, Nucl. Instrum. Methods Phys. Res., Sect. B **175**, 417 (2001).
[26]A. Benyagoub, Nucl. Instrum. Methods Phys. Res., Sect. B **206**, 132 (2003).
[27]A. Benyagoub, Nucl. Instrum. Methods Phys. Res., Sect. B **218**, 451 (2004).
[28]M. Lang, F. Zhang, J. Zhang, C. L. Tracy, A. B. Cusick, J. VonEhr, Z. Chen, C. Trautmann, and R. C. Ewing, Nucl. Instrum. Methods Phys. Res., Sect. B **326**, 121 (2014).
[29]F. Watanabe, D. G. Cahill, B. Gundrum, and R. S. Averback, J. Appl. Phys. **100**, 083519 (2006).
[30]D. Jia, L. Lu, and W. M. Yen, Opt. Commun. **212**, 97 (2002).
[31]R. H. French, S. J. Glass, F. S. Ohuchi, Y.-N. Xu, and W. Y. Ching, Phys. Rev. B **49**, 5133 (1994).
[32]R. Fillit, R. P. Homerin, R. J. Schafer, R. H. Bruyas, and R. F. Thevenot, J. Mater. Sci. **22**, 3566 (1987).
[33]M. G. Krishna, K. N. Rao, and S. Mohan, Appl. Phys. Lett. **57**, 557 (1990).
[34]J. Zarembowitch and J. Gouteron, J. Raman Spectrosc. **9**, 263 (1980).
[35]P. E. Quintard, P. Barbéris, A. P. Mirgorodsky, and T. Merle-Méjean, J. Am. Ceram. Soc. **85**, 1745 (2002).
[36]C. L. Tracy, J. McLain Pray, M. Lang, D. Popov, C. Park, C. Trautmann, and R. C. Ewing, Nucl. Instrum. Methods Phys. Res., Sect. B **326**, 169 (2014).
[37]A. Kumar and T. M. Pollock, J. Appl. Phys. **110**, 083114 (2011).
[38]Q. Feng, Y. N. Picard, H. Liu, S. M. Yalisove, G. Mourou, and T. M. Pollock, Scr. Mater. **53**, 511 (2005).
[39]Q. Feng, Y. N. Picard, J. P. McDonald, P. A. Van Rompay, S. M. Yalisove, and T. M. Pollock, Mater. Sci. Eng., A **430**, 203 (2006).
[40]D. Vanderbilt, X. Zhao, and D. Ceresoli, Thin Solid Films **486**, 125 (2005).
[41]S. Davison, R. Kershaw, K. Dwight, and A. Wold, J. Solid State Chem. **73**, 47 (1988).
[42]P. P. Pronko, P. A. VanRompay, C. Horvath, F. Loesel, T. Juhasz, X. Liu, and G. Mourou, Phys. Rev. B **58**, 2387 (1998).
[43]J. Bonse, K. W. Brzezinka, and A. J. Meixner, Appl. Surf. Sci. **221**, 215 (2004).
[44]A. Vaidyanathan, T. Walker, and A. H. Guenther, IEEE J. Quantum Electron. **16**, 89 (1980).